Department Project II

Project Report

Analyzing the Oscillation spectra of subgiants using machine learning

Department of Astronomy And Astrophysics
Tata Institute of Fundamental Research, Mumbai

Submitted by: **Gursharan Singh**
Supervised by: **Prof Shravan Hanasoge**

Abstract

Subgiants are crucial for studying stellar evolution, as they lie between the main sequence and red giant phases. Asteroseismology is the only technique capable of probing the interiors of such stars. However, the process of fitting the oscillation spectrum to infer stellar parameters is computationally expensive. Traditional methods such as MCMC can take up to a week to converge to the best fit for a single star. With the advent of new space telescopes that generate data at high speeds, it is nearly impossible to analyze all the data using traditional techniques. To address this challenge, we propose a novel machine-learning-based method to infer parameters such as $\Delta\nu$, $\Delta\Pi$, and the coupling factor q. Once trained, our machine-learning model predicts accurate results in seconds, offering a significant advantage over traditional methods. This approach is particularly valuable for future missions such as PLATO, which will generate large datasets.

We trained our model on synthetic data, generated using realistic physics, and validated it using published inferences on Kepler subgiants. Our results show promising agreement, demonstrating the potential of machine learning in asteroseismology for rapid and efficient analysis.

1 Introduction

Asteroseismology is the study of a star's internal structure by measuring and interpreting its oscillations. Much as earthquakes, starquakes carry information about the structure and evolution of the star. These starquakes or stellar oscillations can be produced by many different mechanisms, depending on the type of star. In solar-like stars that contain both a core and an envelope, oscillations are driven by turbulence in the outer layers of the convective zone. Depending upon the restoring force type, there are two oscillatory modes in solar-like stars - p modes, where pressure is the restoring force (similar to acoustic waves) and g modes, where gravity or buoyancy provides the restoring force.

Subgiants are solar-like stars located between the main sequence and the red giant branch on the evolutionary ladder of the Hertzsprung–Russell diagram (figure 1). Studying subgiants is crucial to building our understanding of the evolutionary transition from the main sequence to the red giant phases.

The Kepler mission (2009) recorded the oscillations of numerous subgiants. By analyzing the light curves of these stars and converting them into power spectra (the squared absolute values of the Fourier transforms of the recorded light curves) ordered patterns of peaks were observed. When correctly identified and assigned

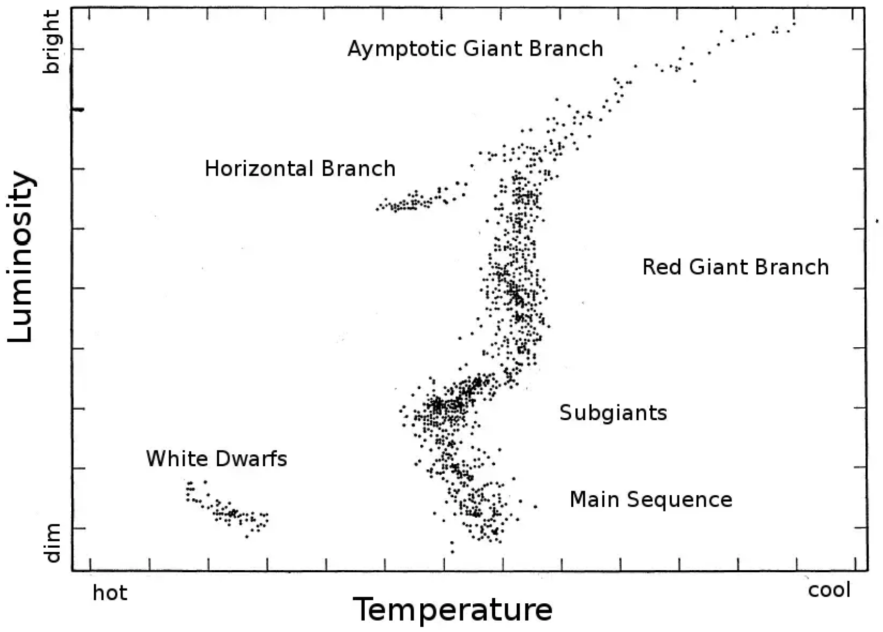

Figure 1: Hertzsprung–Russell diagram

quantum numbers n, ℓ, and m, these patterns provide valuable information about the star, including its radius, density, metallicity, and the rotation rates of both its envelope and core.

2 Theory of Stellar Oscillations

On perturbing the equation of the stellar evolution and retaining only first-order terms, one arrives at the following equation [5]

$$\frac{d^2\xi_r}{dr^2} = \frac{\omega^2}{c_s^2}\left(1 - \frac{N^2}{\omega^2}\right)\left(\frac{S_l^2}{\omega^2} - 1\right)\xi_r \tag{1}$$

where ω^2, N^2, and S_l^2 are the eigenvalue, Brunt-Väisälä frequency, and Lamb frequency, respectively. The radial eigenfunction ξ_r has oscillatory solutions only when the following condition is met

1. $\omega^2 < S_l^2$, and $\omega^2 < N^2$
2. $\omega^2 > S_l^2$, and $\omega^2 > N^2$

Modes that satisfy the first condition are p modes while the modes that satisfy the second condition are g modes. Variations in N^2 and S_l^2 with stellar radius are shown in Figure 2a. These are often referred to as propagation diagrams since they show

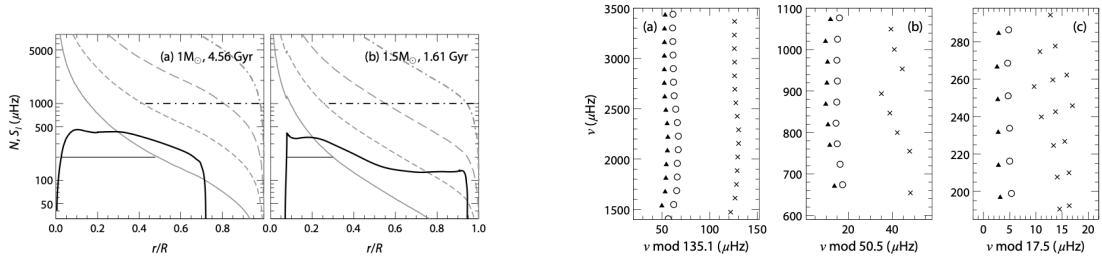

(a) (b)

Figure 2: (a) Wave-propagation diagrams for models of two main-sequence stars. In both panels, the heavy black line represents the Brunt-Väisälä frequency, N. The gray lines represent the Lamb frequency, S, for $\ell = 1$ (solid), $\ell = 5$ (short-dashed line), $\ell = 20$ (long-dashed line), and $\ell = 100$ (dot-dashed line). The dot-dashed horizontal line marks the cavity for a p mode with frequency 1,000 μHz, while the solid horizontal line marks the cavity for a 200 μHz g mode. (b) Échelle diagrams for the Sun (left panel), subgiant KIC 11026764 (middle panel), and the red giant KIC 6448890 (Kepler 56; right panel). Circles denote $\ell = 0$ modes, triangles represent $\ell = 2$ modes, and crosses correspond to $\ell = 1$ modes.

where different modes can propagate in the stellar interior. The figure shows that the modes for which the first condition is true (i.e. $\omega^2 < S_l^2$ and $\omega^2 < N^2$) are trapped mainly in the inner regions. These are the g modes, whose restoring force is gravity. Modes that satisfy the second condition (i.e. $\omega^2 > S_l^2$ and $\omega^2 > N^2$) are oscillatory in the outer regions, though low-degree modes can penetrate right to the core. These are the p modes, whose restoring force is provided by the gradient of the pressure.

The figure 2a also shows that modes of different degrees sample different layers of a star. For a given degree, higher frequency modes penetrate deeper into a star.

2.1 Asymptotic Properties of p and g Mode

2.1.1 P modes

The frequency relation [2] may be expressed as:

$$\nu_{n,\ell} = \Delta\nu \left(n + \frac{\ell}{2} + p \right) - \ell(\ell+1) D_0 \tag{2}$$

where $\Delta\nu$ is the large frequency separation, D_0 is the small frequency separation, and p is the offset parameter with $D_0 \ll \Delta\nu$.
Key characteristics of p-modes include:

- Frequency peaks (or resonances) of p-modes [6] of the same degree (ℓ) are approximately evenly spaced by $\Delta\nu$ as shown in the figure 4.
- Peaks corresponding to $\ell = 0$ and $\ell = 2$ are located close to each other, with a separation of $6D_0$, as explained by Equation 2. Similarly, the peaks for $\ell = 1$ and $\ell = 3$ are also closely spaced, which we see in figure 4.

2.1.2 G modes

These are buoyancy fluctuations with gravity serving as the restoring force, making them low-frequency modes. They are trapped deep inside the core of the star and as a result, are not visible at the surface and therefore absent from the observed power spectrum. While p-modes are spaced equally in frequency, g-modes are spaced equally in period, with the period spacing given by:

$$\Delta\Pi_\ell = \frac{\Delta\Pi_0}{L} \tag{3}$$

where

$$\Delta\Pi_0 = 2\pi^2 \left(\int_{r_1}^{r_2} N \frac{dr}{r} \right)^{-1} \tag{4}$$

2.1.3 Mixed p/g modes

These behave like g modes in the core and p modes in the convective zone of the star. Owing to this property, they contain information about the interior of the star. The frequencies of the mixed modes are asymptotically given by the solutions of the equation:

$$\tan\left(\pi \frac{\nu - \nu_p}{\Delta\nu}\right) = q \tan\left(\frac{\pi}{\Delta\Pi}\left(\frac{1}{\nu} - \frac{1}{\nu_g}\right)\right) \tag{5}$$

where q is the coupling factor. Here, $\nu_p \approx \Delta\nu \left(n_p + \frac{1}{2} + p\right) - 2D_0$ and $\frac{1}{\nu_g} = (-n_g + g)\Delta\Pi$ and the coupling constant q is given by:

$$q = \frac{1}{4} \exp\left(-2 \int_{r_b}^{r_c} |K(r)|^{1/2} \; dr\right) \tag{6}$$

where r_b and r_c are the boundaries of the relevant region, and $K(r)$ is the corresponding function.

2.2 Effect of Rotation

Stellar rotation breaks the assumption of spherical symmetry, thereby lifting the degeneracy of modes with respect to m [i.e. it now has $2\ell + 1$ modes in m]. If the rotation is sufficiently slow, we can use perturbation theory to predict its effect.

When a star undergoes solid-body rotation at an angular rate Ω, the frequency of each mode, denoted as $\nu_{n,\ell,m}$ may be expressed as:

$$\nu_{n,\ell,m} = \nu_{n,\ell} + \delta\nu_{n,\ell,m}$$

where the rotational splitting $\delta\nu_{n,\ell,m}$ is given by:

$$\delta\nu_{n,\ell,m} = m\,(C_{n,\ell} - 1)\,\Omega$$

For pressure (p) modes, the Ledoux constant $C_{n,\ell} \approx 0$, and for gravity (g) modes, $C_{n,\ell} \approx \frac{1}{\ell(\ell+1)}$. As a result, the frequency multiplets of p-modes are approximated by:

$$\nu_{n,\ell,m} = \nu_{n,\ell} - m\nu_s$$

where ν_s is proportional to the stellar rotation rate and is called splitting frequency.

2.3 Visibility

The observations correspond to integrals over the visible stellar disc, because of which contributions from small-scale modes [i.e. high-degree modes] vanish due to the cancellation effect shown in Figure 3b. We can only measure high-degree modes in the Sun because its surface is resolved.

The observed amplitude may be expressed as:

$$a_{n,\ell,m} = r_{\ell,m}(i)V_\ell A \tag{7}$$

where V_ℓ is called the mode visibility, $r_{\ell,m}(i)$ is the relative amplitude of the mode inside a multiplet and depends only on the inclination angle i between the rotation axis and the line of sight as shown in the figure 3a.

Mode visibilities may be written as:

$$V_\ell = \sqrt{(2\ell+1)\pi} \int_0^1 P_\ell(\mu) W(\mu) \mu \, d\mu \tag{8}$$

where P_ℓ is the ℓth order Legendre polynomial, and $W(\mu)$ is a weighting function depending only on the distance to the limb μ. When V_ℓ depends on the stellar atmosphere and the instrument, the factor $r_{\ell,m}(i)$ is purely geometric and reads:

$$r^2_{\ell,m}(i) = \frac{(\ell - |m|)!}{(\ell + |m|)!} \left[P_\ell^{|m|}(\cos i) \right]^2$$

where $P_\ell^{|m|}$ are the associated Legendre functions. Figure 3a shows the variation of these coefficients with i for $\ell = 1$ and $\ell = 2$. The squared factor $r^2_{\ell,m}(i)$ represents the relative power of modes in a multiplet. We notice that $\sum_m r^2_{\ell,m}(i) = 1$.

For stars observed pole-on ($i = 0°$), only axisymmetric ($m = 0$) modes are visible; it is not possible to infer the rotation rate in this case. For stars observed equator-on ($i = 90°$), only components with even $\ell + m$ are visible.

3 Spectral Analysis

We present an example of an observed power spectrum in Figure 4. To analyze this spectrum, we employ an alternative representation known as the échelle diagram (see Figure 2b). In the échelle diagram, the $l = 1$ mixed modes can be identified as those deviating from the common frequency pattern and not aligning as straight lines like the $l = 0$ and $l = 2$ modes. This phenomenon is referred to as avoided crossing. Additionally, the $l = 2$ rotational splittings are visible in Figure 4.

4 Asteroseismic Scaling Relations

It can be shown [5] that the masses and radii of stars may be expressed as functions of the seismic variables $\nu_{\max}$ and $\Delta\nu$, assuming that T_{eff} is known from photometry

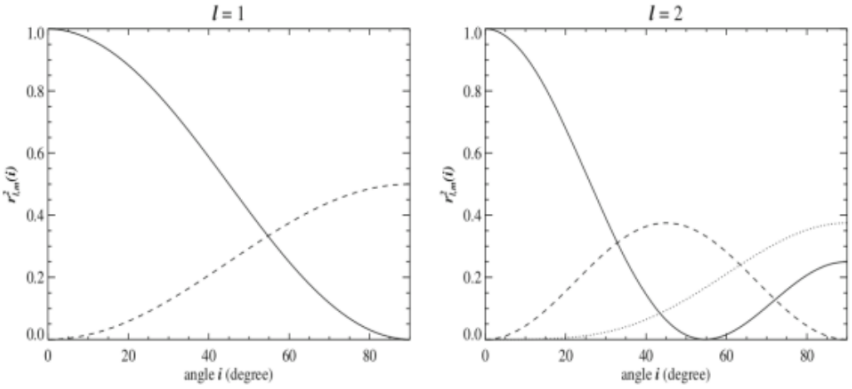

(a)

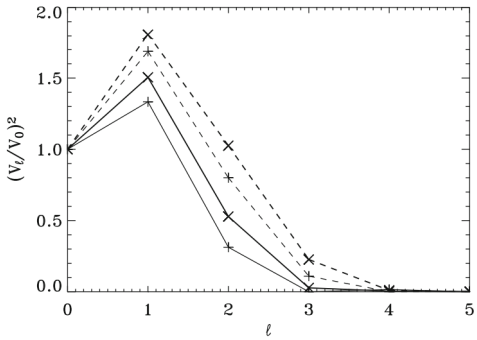

(b)

Figure 3: (a) Relative amplitude variation with the inclination angle i (b) Mode visibilities V_l as a function of the degree l.

or spectroscopy.

$$R \approx R_{\odot} \left(\frac{\nu_{\max}}{\nu_{\max\odot}}\right) \left(\frac{\Delta\nu}{\Delta\nu_{\odot}}\right)^{-2} \left(\frac{T_{\rm eff}}{T_{\rm eff\odot}}\right)^{1/2} \tag{9}$$

$$M \approx M_{\odot} \left(\frac{\nu_{\max}}{\nu_{\max\odot}}\right)^{3} \left(\frac{\Delta\nu}{\Delta\nu_{\odot}}\right)^{-4} \left(\frac{T_{\rm eff}}{T_{\rm eff\odot}}\right)^{3/2} \tag{10}$$

These scaling relations provide an efficient method with which to estimate stellar masses and radii without requiring detailed stellar models. The precision of these estimates depends mainly on the accuracies of the measurements of $\nu_{\max}$ and $\Delta\nu$.

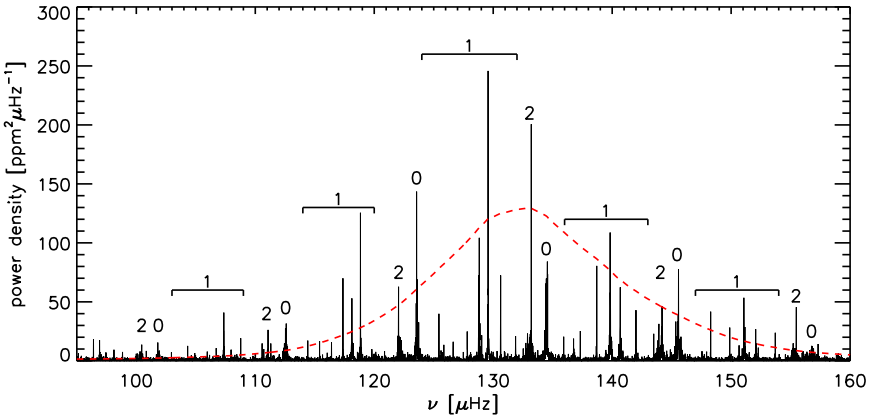

Figure 4: Oscillation spectrum of red giant star KIC 9145955. Here, $l = 0$, 2 frequency resonances are p modes and $l = 1$ resonances are mixed modes of oscillation.

5 Machine learning

5.1 Machine learning model

This analysis uses a CNN-LSTM hybrid Model [4] [7]. The model architecture is shown in Figure 5.

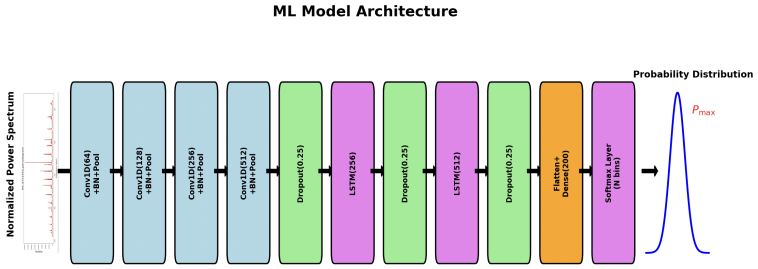

Figure 5: Architecture of the model used in the analysis.

The normalized power spectrum is fed into the model as an image. The CNN (Convolutional Neural Network) first identifies patterns under translational symmetry and passes this information to the LSTM (Long Short-Term Memory) network, which recognizes sequential patterns in the dataset. The model outputs the probability associated with each bin of the seismic parameter. By binning the expected range of the output parameters, we have effectively transformed this regression task into

a classification problem. Finally, the bin with the highest probability is selected as the value of the output parameter. The figure 6 shows the variation of training and validation loss with the number of epochs. This helps in understanding the training process and determining whether the model is underfitting or overfitting.

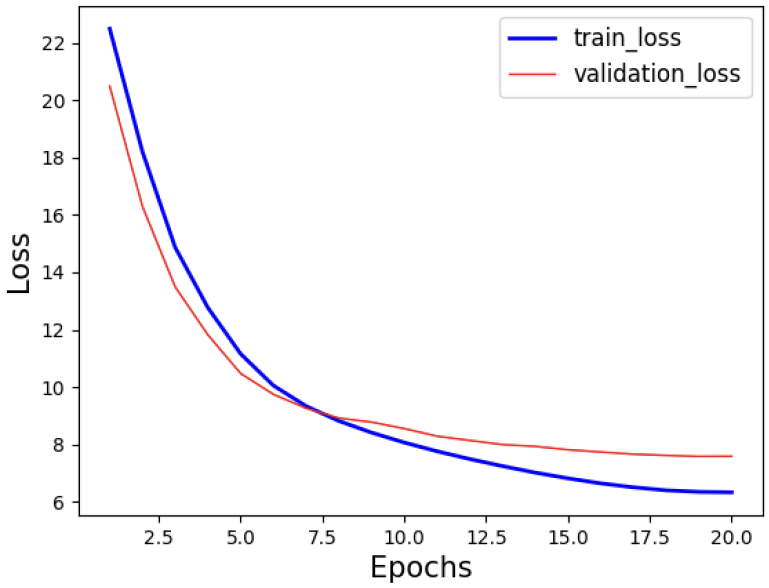

Figure 6: Training and Validation loss variation with number of Epoch.

6 Results on Synthetics

We built datasets using a simulator available at Spectra Simulator on GitHub that can generate synthetic spectra over a wider range of parameters. The software incorporates the physics of the structure, composition gradient, and rotation in red giants using the asymptotic theory of stellar oscillations [5].

We have generated 1,024,000 samples of synthetic subgiant oscillation spectra using different ranges of parameters described in [1] [9]. We split the synthetics into 64000 instances for validation and 64000 for testing and use the remaining for training (896000).

The results for inferences of $\Delta\nu$, $\Delta\pi$ and q are given in Figure 7a, Figure 7b and Figure 7c respectively. We have obtained a validation accuracy of $\Delta\nu$, $\Delta\Pi$, q as 84.5%, 63.4%, and 54.1% respectively. Figure 7d once again confirms the validity of our training process, as we have generated synthetics with uniform $\Delta\nu$ and $\Delta\pi$.

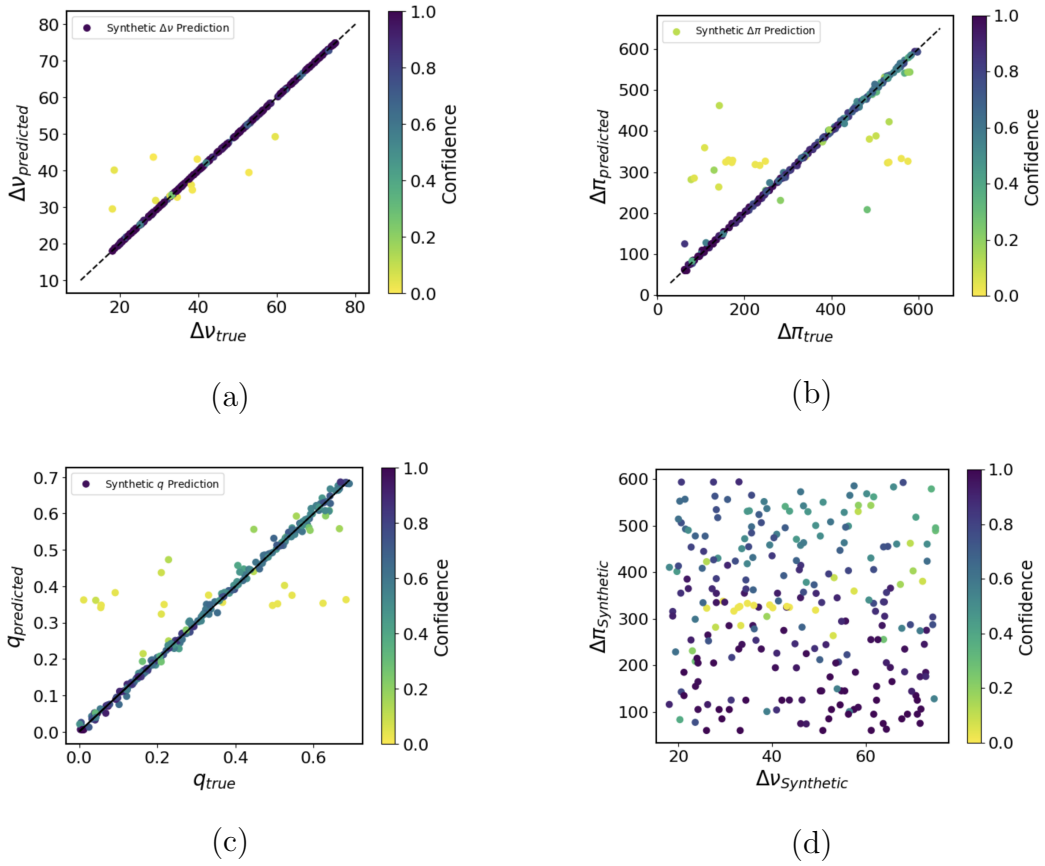

Figure 7: (a) $\Delta\nu$ predicted vs $\Delta\nu$ true, (b) $\Delta\Pi$ predicted vs $\Delta\Pi$ True, (c) q predicted vs q true, and (d) $\Delta\Pi$ predicted vs $\Delta\nu$ predicted.

7 Results on observations

We obtained observations of subgiants that have already been published [8] [3] and plotted our machine-predicted values of $\Delta\nu$ and $\Delta\pi$ as given in Figures 8a and 8b respectively.

The model predicts the relation between $\Delta\nu$ and $\Delta\pi$ for these published subgiant stars (figure 8d). Additionally, $\Delta\nu$ and q also appear to be correlated, suggesting a deeper evolutionary connection between them (figure 8c).

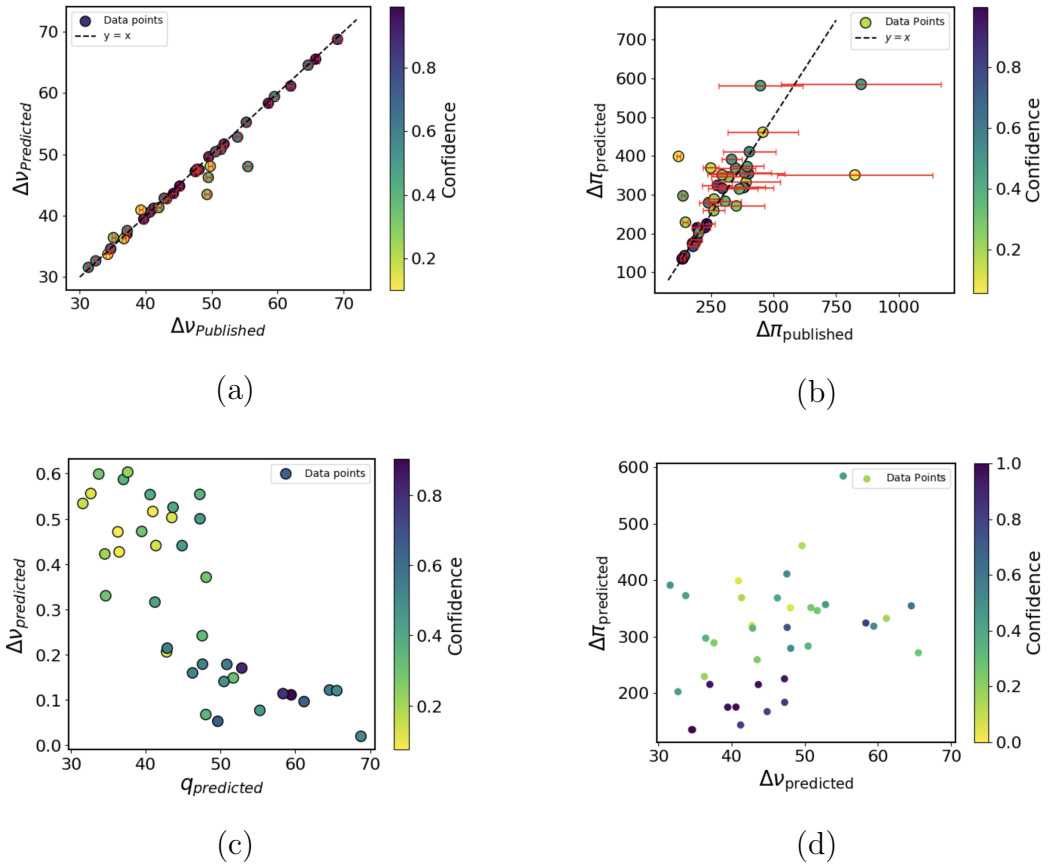

Figure 8: Diagrams showing the variations in different parameters: (a) $\Delta\nu$ predicted vs $\Delta\nu$ published, (b) $\Delta\pi$ predicted vs $\Delta\pi$ published, (c) $\Delta\nu$ predicted vs q predicted (d) $\Delta\nu$ predicted vs $\Delta\pi$ predicted .

8 Acknowledgement

I would like to express my heartfelt gratitude to Prof. Shravan Hanasoge for his invaluable guidance and support throughout every step of this project. I am also deeply thankful to Dr. Meenakshi Gaira for her assistance and understanding, which greatly helped me during this work.

Additionally, I wish to thank Shatanik, Rajarshi, and Anoop for their insightful discussions on the theory of asteroseismology, which enriched my understanding of the subject. Finally, I am grateful to Anilkumar Naik, who manages the HPC facility at TIFR Mumbai, for providing computational resources.

References

[1] O. Benomar, T. R. Bedding, D. Stello, S. Deheuvels, T. R. White, and J. Christensen-Dalsgaard. Masses of subgiant stars from asteroseismology using the coupling strengths of mixed modes. *Astrophys. J. Lett.*, 745:L33, 2012.

[2] Tiago L. Campante. *An Introduction to Data Analysis in Asteroseismology*, page 55–74. Springer International Publishing, July 2017.

[3] Miguel Clara, Margarida S. Cunha, Pedro P. Avelino, Tiago L. Campante, Sébastien Deheuvels, and Daniel R. Reese. On the seismic modelling of subgiant stars: testing different grid interpolation methods. 2025.

[4] Siddharth Dhanpal, Othman Benomar, Shravan Hanasoge, Abhisek Kundu, Dattaraj Dhuri, Dipankar Das, and Bharat Kaul. Measuring frequency and period separations in red-giant stars using machine learning. *The Astrophysical Journal*, 928(2):188, April 2022.

[5] Rafael A. García and Jérôme Ballot. Asteroseismology of solar-type stars. *Living Reviews in Solar Physics*, 16(1):4, 2019.

[6] Saskia Hekker and Anwesh Mazumdar. Solar-like oscillations in subgiant and red-giant stars: mixed modes. *Proceedings of the International Astronomical Union*, 9(S301):325–331, 2013.

[7] Marc Hon, Earl P Bellinger, Saskia Hekker, Dennis Stello, and James S Kuszlewicz. Asteroseismic inference of subgiant evolutionary parameters with deep learning. *Monthly Notices of the Royal Astronomical Society*, 499(2):2445–2461, September 2020.

[8] B. Mosser, O. Benomar, K. Belkacem, M. J. Goupil, N. Lagarde, E. Michel, Y. Lebreton, D. Stello, M. Vrard, C. Barban, T. R. Bedding, S. Deheuvels, W. J. Chaplin, J. De Ridder, Y. Elsworth, J. Montalban, A. Noels, R. M. Ouazzani, R. Samadi, T. R. White, and H. Kjeldsen. Mixed modes in red giants: a window on stellar evolution. *Astronomy amp; Astrophysics*, 572:L5, November 2014.

[9] Tian, Zhijia, Bi, Shaolan, Bedding, Timothy R., and Yang, Wuming. Asteroseismic analysis of solar-mass subgiants kic 6442183 and kic 11137075 observed by kepler. *AA*, 580:A44, 2015.